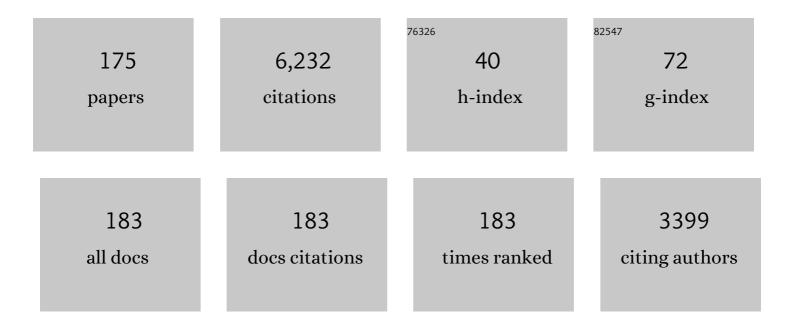
List of Publications by Year in descending order

Source: https://exaly.com/author-pdf/515005/publications.pdf Version: 2024-02-01



SEUL SUCITA

#	Article	IF	CITATIONS
1	Samples returned from the asteroid Ryugu are similar to Ivuna-type carbonaceous meteorites. Science, 2023, 379, .	12.6	97
2	Resurfacing processes constrained by crater distribution on Ryugu. Icarus, 2022, 377, 114911.	2.5	6
3	Mid-infrared emissivity of partially dehydrated asteroid (162173) Ryugu shows strong signs of aqueous alteration. Nature Communications, 2022, 13, 364.	12.8	10
4	Pebbles and sand on asteroid (162173) Ryugu: In situ observation and particles returned to Earth. Science, 2022, 375, 1011-1016.	12.6	78
5	Three-axial shape distributions of pebbles, cobbles and boulders smaller than a few meters on asteroid Ryugu. Icarus, 2022, 381, 115007.	2.5	1
6	Preliminary analysis of the Hayabusa2 samples returned from C-type asteroid Ryugu. Nature Astronomy, 2022, 6, 214-220.	10.1	136
7	First compositional analysis of Ryugu samples by the MicrOmega hyperspectral microscope. Nature Astronomy, 2022, 6, 221-225.	10.1	65
8	Mission objectives, planning, and achievements of Hayabusa2. , 2022, , 5-23.		3
9	Sensitivity degradation of optical navigation camera and attempts for dust removal. , 2022, , 415-431.		1
10	Site selection for the Hayabusa2 artificial cratering and subsurface material sampling on Ryugu. Planetary and Space Science, 2022, 219, 105519.	1.7	4
11	The ESA Hera Mission: Detailed Characterization of the DART Impact Outcome and of the Binary Asteroid (65803) Didymos. Planetary Science Journal, 2022, 3, 160.	3.6	82
12	Utilization of a meteorological satellite as a space telescope: the lunar mid-infrared spectrum as seen by Himawari-8. Earth, Planets and Space, 2022, 74, .	2.5	0
13	Spacecraft sample collection and subsurface excavation of asteroid (101955) Bennu. Science, 2022, 377, 285-291.	12.6	39
14	Crater depth-to-diameter ratios on asteroid 162173 Ryugu. Icarus, 2021, 354, 114016.	2.5	12
15	Spectral characterization of the craters of Ryugu as observed by the NIRS3 instrument on-board Hayabusa2. Icarus, 2021, 357, 114253.	2.5	7
16	Ballistic deployment of the Hayabusa2 artificial landmarks in the microgravity environment of Ryugu. Icarus, 2021, 358, 114220.	2.5	13
17	Experimental study concerning the oblique impact of low- and high-density projectiles on sedimentary rocks. Planetary and Space Science, 2021, 195, 105141.	1.7	6
18	Collisional history of Ryugu's parent body from bright surface boulders. Nature Astronomy, 2021, 5, 39-45.	10.1	42

#	Article	IF	CITATIONS
19	Thermally altered subsurface material of asteroid (162173) Ryugu. Nature Astronomy, 2021, 5, 246-250.	10.1	47
20	Alignment determination of the Hayabusa2 laser altimeter (LIDAR). Earth, Planets and Space, 2021, 73, .	2.5	3
21	Simulation of Seismic Wave Propagation on Asteroid Ryugu Induced by The Impact Experiment of The Hayabusa2 Mission: Limited Mass Transport by Low Yield Strength of Porous Regolith. Journal of Geophysical Research E: Planets, 2021, 126, e2020JE006594.	3.6	8
22	Spectrophotometric Analysis of the Ryugu Rock Seen by MASCOT: Searching for a Carbonaceous Chondrite Analog. Planetary Science Journal, 2021, 2, 58.	3.6	7
23	Numerical modeling of lander interaction with a low-gravity asteroid regolith surface. Astronomy and Astrophysics, 2021, 648, A56.	5.1	10
24	Post-arrival calibration of Hayabusa2's optical navigation cameras (ONCs): Severe effects from touchdown events. Icarus, 2021, 360, 114353.	2.5	11
25	Anomalously porous boulders on (162173) Ryugu as primordial materials from its parent body. Nature Astronomy, 2021, 5, 766-774.	10.1	30
26	Improved method of hydrous mineral detection by latitudinal distribution of 0.7-μm surface reflectance absorption on the asteroid Ryugu. Icarus, 2021, 360, 114348.	2.5	9
27	Geologic History and Crater Morphology of Asteroid (162173) Ryugu. Journal of Geophysical Research E: Planets, 2021, 126, e2020JE006572.	3.6	10
28	Optical design adopting tilted filters for reduction of stray light in planetary exploration cameras and other optics. , 2021, , .		0
29	Hayabusa2 extended mission: New voyage to rendezvous with a small asteroid rotating with a short period. Advances in Space Research, 2021, 68, 1533-1555.	2.6	20
30	Rotational states and shapes of Ryugu and Bennu: Implications for interior structure and strength. Planetary and Space Science, 2021, 204, 105268.	1.7	15
31	Resurfacing processes on asteroid (162173) Ryugu caused by an artificial impact of Hayabusa2's Small Carry-on Impactor. Icarus, 2021, 366, 114530.	2.5	24
32	Opposition Observations of 162173 Ryugu: Normal Albedo Map Highlights Variations in Regolith Characteristics. Planetary Science Journal, 2021, 2, 177.	3.6	12
33	Development of image texture analysis technique for boulder distribution measurements: Applications to asteroids Ryugu and Itokawa. Planetary and Space Science, 2021, 204, 105249.	1.7	6
34	Hayabusa2 pinpoint touchdown near the artificial crater on Ryugu: Trajectory design and guidance performance. Advances in Space Research, 2021, 68, 3093-3140.	2.6	9
35	High-resolution observations of bright boulders on asteroid Ryugu: 1. Size frequency distribution and morphology. Icarus, 2021, 369, 114529.	2.5	2
36	High-resolution observations of bright boulders on asteroid Ryugu: 2. Spectral properties. Icarus, 2021, 369, 114591.	2.5	5

#	Article	IF	CITATIONS
37	Spectrally blue hydrated parent body of asteroid (162173) Ryugu. Nature Communications, 2021, 12, 5837.	12.8	23
38	YORP Effect on Asteroid 162173 Ryugu: Implications for the Dynamical History. Journal of Geophysical Research E: Planets, 2021, 126, e2021JE006863.	3.6	4
39	The spatial distribution of impact craters on Ryugu. Icarus, 2020, 338, 113527.	2.5	25
40	Hayabusa2 Landing Site Selection: Surface Topography of Ryugu and Touchdown Safety. Space Science Reviews, 2020, 216, 1.	8.1	17
41	Variations in color and reflectance on the surface of asteroid (101955) Bennu. Science, 2020, 370, .	12.6	84
42	Ne-Ar separation using a permeable membrane to measure Ne isotopes for future planetary explorations. Planetary and Space Science, 2020, 193, 105046.	1.7	1
43	Spin-driven evolution of asteroids' top-shapes at fast and slow spins seen from (101955) Bennu and (162173) Ryugu. Icarus, 2020, 352, 113946.	2.5	28
44	Motion reconstruction of the small carry-on impactor aboard Hayabusa2. Astrodynamics, 2020, 4, 289-308.	2.4	7
45	Macroporosity and Grain Density of Rubble Pile Asteroid (162173) Ryugu. Journal of Geophysical Research E: Planets, 2020, 125, e2020JE006519.	3.6	27
46	Global photometric properties of (162173) Ryugu. Astronomy and Astrophysics, 2020, 639, A83.	5.1	37
47	Surface roughness of asteroid (162173) Ryugu and comet 67P/Churyumov–Gerasimenko inferred from <i>in situ</i> observations. Monthly Notices of the Royal Astronomical Society, 2020, 500, 3178-3193.	4.4	11
48	Sample collection from asteroid (162173) Ryugu by Hayabusa2: Implications for surface evolution. Science, 2020, 368, 654-659.	12.6	158
49	Collisional formation of top-shaped asteroids and implications for the origins of Ryugu and Bennu. Nature Communications, 2020, 11, 2655.	12.8	87
50	Thermophysical properties of the surface of asteroid 162173 Ryugu: Infrared observations and thermal inertia mapping. Icarus, 2020, 348, 113835.	2.5	48
51	Design and Reconstruction of the Hayabusa2 Precision Landing on Ryugu. Journal of Spacecraft and Rockets, 2020, 57, 1033-1060.	1.9	20
52	Hayabusa2's kinetic impact experiment: Operational planning and results. Acta Astronautica, 2020, 175, 362-374.	3.2	14
53	Highly porous nature of a primitive asteroid revealed by thermal imaging. Nature, 2020, 579, 518-522.	27.8	100
54	An artificial impact on the asteroid (162173) Ryugu formed a crater in the gravity-dominated regime. Science, 2020, 368, 67-71.	12.6	183

#	Article	IF	CITATIONS
55	Impact Experiment on Asteroid (162173) Ryugu: Structure beneath the Impact Point Revealed by In Situ Observations of the Ejecta Curtain. Astrophysical Journal Letters, 2020, 899, L22.	8.3	19
56	Images from the surface of asteroid Ryugu show rocks similar to carbonaceous chondrite meteorites. Science, 2019, 365, 817-820.	12.6	99
57	Multivariable statistical analysis of spectrophotometry and spectra of (162173) Ryugu as observed by JAXA Hayabusa2 mission. Astronomy and Astrophysics, 2019, 629, A13.	5.1	15
58	Updated inflight calibration of Hayabusa2's optical navigation camera (ONC) for scientific observations during the cruise phase. Icarus, 2019, 325, 153-195.	2.5	48
59	Boulder size and shape distributions on asteroid Ryugu. Icarus, 2019, 331, 179-191.	2.5	107
60	Shape of (101955) Bennu indicative of a rubble pile with internal stiffness. Nature Geoscience, 2019, 12, 247-252.	12.9	179
61	The surface composition of asteroid 162173 Ryugu from Hayabusa2 near-infrared spectroscopy. Science, 2019, 364, 272-275.	12.6	262
62	Hayabusa2 arrives at the carbonaceous asteroid 162173 Ryugu—A spinning top–shaped rubble pile. Science, 2019, 364, 268-272.	12.6	410
63	The geomorphology, color, and thermal properties of Ryugu: Implications for parent-body processes. Science, 2019, 364, 252.	12.6	313
64	The Western Bulge of 162173 Ryugu Formed as a Result of a Rotationally Driven Deformation Process. Astrophysical Journal Letters, 2019, 874, L10.	8.3	30
65	The MASCOT landing area on asteroid (162173) Ryugu: Stereo-photogrammetric analysis using images of the ONC onboard the Hayabusa2 spacecraft. Astronomy and Astrophysics, 2019, 632, L4.	5.1	9
66	The Hayabusa2 lander MASCOT on the surface of asteroid (162173) Ryugu – Stereo-photogrammetric analysis of MASCam image data. Astronomy and Astrophysics, 2019, 632, L5.	5.1	14
67	The descent and bouncing path of the Hayabusa2 lander MASCOT at asteroid (162173) Ryugu. Astronomy and Astrophysics, 2019, 632, L3.	5.1	18
68	Experimental study of heterogeneous organic chemistry induced by far ultraviolet light: Implications for growth of organic aerosols by CH3 addition in the atmospheres of Titan and early Earth. Icarus, 2018, 307, 25-39.	2.5	3
69	Vis-NIR disk-integrated photometry of asteroid 25143 Itokawa around opposition by AMICA/Hayabusa. Icarus, 2018, 311, 175-196.	2.5	15
70	Ground-based characterization of Hayabusa2 mission target asteroid 162173 Ryugu: constraining mineralogical composition in preparation for spacecraft operations. Monthly Notices of the Royal Astronomical Society, 2018, 475, 614-623.	4.4	21
71	Initial inflight calibration for Hayabusa2 optical navigation camera (ONC) for science observations of asteroid Ryugu. Icarus, 2018, 300, 341-359.	2.5	56
72	Cratering efficiency on coarse-grain targets: Implications for the dynamical evolution of asteroid 25143 Itokawa. Icarus, 2018, 300, 227-248.	2.5	48

#	Article	IF	CITATIONS
73	Spectral decomposition of asteroid Itokawa based on principal component analysis. Icarus, 2018, 299, 386-395.	2.5	7
74	Numerical modeling of lander interaction with a low-gravity asteroid regolith surface. Astronomy and Astrophysics, 2018, 615, A41.	5.1	31
75	Reflectance spectra of Asteroids and Meteorites: their classifications and statistical comparisons. Journal of Physics: Conference Series, 2018, 1036, 012003.	0.4	3
76	Quantitative Potassium Measurements with Laser-Induced Breakdown Spectroscopy Using Low-Energy Lasers: Application to In Situ K–Ar Geochronology for Planetary Exploration. Applied Spectroscopy, 2017, 71, 1969-1981.	2.2	7
77	Preflight Calibration Test Results for Optical Navigation Camera Telescope (ONC-T) Onboard the Hayabusa2 Spacecraft. Space Science Reviews, 2017, 208, 17-31.	8.1	81
78	High Pressure Experiments on Metalâ€5ilicate Partitioning of Chlorine in a Magma Ocean: Implications for Terrestrial Chlorine Depletion. Geochemistry, Geophysics, Geosystems, 2017, 18, 3929-3945.	2.5	8
79	Experimental characterization of elastomeric O-rings as reusable seals for mass spectrometric measurements: Application to in situ K–Ar dating on Mars. Advances in Space Research, 2017, 60, 1453-1462.	2.6	2
80	The Camera of the MASCOT Asteroid Lander on Board Hayabusa 2. Space Science Reviews, 2017, 208, 375-400.	8.1	46
81	Ecliptic North outh Symmetry of Hydrogen Geocorona. Geophysical Research Letters, 2017, 44, 11,706.	4.0	30
82	Conceptual Design of an In Situ K-Ar Isochron Dating Instrument for Future Mars Rover Missions. Transactions of the Japan Society for Aeronautical and Space Sciences Aerospace Technology Japan, 2016, 14, Pk_89-Pk_94.	0.2	2
83	Cluster analysis on the bulk elemental compositions of Antarctic stony meteorites. Meteoritics and Planetary Science, 2016, 51, 906-919.	1.6	6
84	Shock compression response of forsterite above 250 GPa. Science Advances, 2016, 2, e1600157.	10.3	21
85	An in-situ K–Ar isochron dating method for planetary landers using a spot-by-spot laser-ablation technique. Planetary and Space Science, 2016, 128, 14-29.	1.7	16
86	The Camera of the MASCOT Asteroid Lander on Board Hayabusa 2. , 2016, , 375-400.		3
87	Preflight Calibration Test Results for Optical Navigation Camera Telescope (ONC-T) Onboard the Hayabusa2 Spacecraft. , 2016, , 17-31.		0
88	Dynamics of hypervelocity jetting during oblique impacts of spherical projectiles investigated via ultrafast imaging. Journal of Geophysical Research E: Planets, 2015, 120, 1237-1251.	3.6	33
89	Crater-ray formation by impact-induced ejecta particles. Icarus, 2015, 250, 215-221.	2.5	18
90	High-precision potassium measurements using laser-induced breakdown spectroscopy under high vacuum conditions for in situ K–Ar dating of planetary surfaces. Spectrochimica Acta, Part B: Atomic Spectroscopy, 2015, 106, 28-35.	2.9	17

#	Article	IF	CITATIONS
91	The relative timing of Lunar Magma Ocean solidification and the Late Heavy Bombardment inferred from highly degraded impact basin structures. Icarus, 2015, 250, 492-503.	2.5	30
92	The molecular composition of impact-generated atmospheres on terrestrial planets during the post-accretion stage. Icarus, 2015, 257, 290-301.	2.5	19
93	Detectability of hydrous minerals using ONC-T camera onboard the Hayabusa2 spacecraft. Advances in Space Research, 2015, 56, 1519-1524.	2.6	21
94	Crater Outflow (Venus). , 2015, , 424-428.		0
95	Production of sulphate-rich vapour during the Chicxulub impact and implications for ocean acidification. Nature Geoscience, 2014, 7, 279-282.	12.9	57
96	Gas recovery experiments to determine the degree of shock-induced devolatilization of calcite. Journal of Physics: Conference Series, 2014, 500, 062001.	0.4	4
97	Visible-wavelength spectroscopy of subkilometer-sized near-Earth asteroids with a low delta- <i>v</i> . Publication of the Astronomical Society of Japan, 2014, 66, .	2.5	17
98	Impact chemistry of methanol: Implications for volatile evolution on icy satellites and dwarf planets, and cometary delivery to the Moon. Icarus, 2014, 243, 39-47.	2.5	6
99	Hayabusa2: Scientific importance of samples returned from C-type near-Earth asteroid (162173) 1999 JU3. Geochemical Journal, 2014, 48, 571-587.	1.0	103
100	Hydrogen Cyanide Production due to Mid-Size Impacts in a Redox-Neutral N2-Rich Atmosphere. Origins of Life and Evolution of Biospheres, 2013, 43, 221-245.	1.9	27
101	Viscoelastic deformation of lunar impact basins: Implications for heterogeneity in the deep crustal paleoâ€thermal state and radioactive element concentration. Journal of Geophysical Research E: Planets, 2013, 118, 398-415.	3.6	22
102	Influence of a Polyimide Surface Layer on the Piezoelectric Response of Lead–Zirconate–Titanate Cosmic Dust Detector. Japanese Journal of Applied Physics, 2013, 52, 028002.	1.5	3
103	Dust detector using piezoelectric lead zirconate titanate with current-to-voltage converting amplifier for functional advancement. Earth, Planets and Space, 2013, 65, 167-173.	2.5	2
104	Evaluation of capillary-induced deformation of thin plates due to liquid column formation. Applied Physics Letters, 2013, 103, 043113.	3.3	3
105	Oxidation of carbon compounds by silica-derived oxygen within impact-induced vapor plumes. Earth, Planets and Space, 2013, 65, 811-822.	2.5	8
106	Flyer acceleration experiments using high-power laser. EPJ Web of Conferences, 2013, 59, 19002.	0.3	1
107	Position-Dependent Behavior of Piezoelectric Lead–Zirconate–Titanate Cosmic Dust Detector. Japanese Journal of Applied Physics, 2012, 51, 098004.	1.5	2
108	Direct measurement of chemical composition of SOx in impact vapor using a laser gun. , 2012, , .		2

#	Article	IF	CITATIONS
109	Flyer acceleration by high-power laser and impact experiments at velocities higher than 10 km/s. , 2012, , .		1
110	Time-resolved spectroscopic observations of shockinduced silicate ionization. AIP Conference Proceedings, 2012, , .	0.4	4
111	Young mare volcanism in the Orientale region contemporary with the Procellarum KREEP Terrane (PKT) volcanism peak period â^1⁄42 billion years ago. Geophysical Research Letters, 2012, 39, .	4.0	22
112	A semi-analytical on-hugoniot eos of condensed matter using a linear UP-Us relation. AIP Conference Proceedings, 2012, , .	0.4	8
113	The nature of shock-induced calcite (CaCO3) devolatilization in an open system investigated using a two-stage light gas gun. Earth and Planetary Science Letters, 2012, 337-338, 68-76.	4.4	21
114	A new spectral calculation scheme for longâ€ŧerm deformation of Maxwellian planetary bodies. Journal of Geophysical Research, 2012, 117, .	3.3	10
115	Shockâ€induced silicate vaporization: The role of electrons. Journal of Geophysical Research, 2012, 117, .	3.3	16
116	Laboratory experiments on crater scalingâ€law for sedimentary rocks in the strength regime. Journal of Geophysical Research, 2012, 117, .	3.3	14
117	LCROSS (Lunar Crater Observation and Sensing Satellite) Observation Campaign: Strategies, Implementation, and Lessons Learned. Space Science Reviews, 2012, 167, 93-140.	8.1	19
118	Bayesian spectral deconvolution with the exchange Monte Carlo method. Neural Networks, 2012, 28, 82-89.	5.9	92
119	Investigation of Martian Dust Sample Capture toward Mars Aero-flyby Sample Collection Mission. Transactions of the Japan Society for Aeronautical and Space Sciences Aerospace Technology Japan, 2012, 10, Pk_11-Pk_17.	0.2	5
120	Position-Dependent Behavior of Piezoelectric Lead–Zirconate–Titanate Cosmic Dust Detector. Japanese Journal of Applied Physics, 2012, 51, 098004.	1.5	1
121	Multi-element analysis technique for in-situ planetary exploration by laser-induced breakdown spectroscopy. , 2011, , .		0
122	Replacement and late formation of atmospheric N2 on undifferentiated Titan by impacts. Nature Geoscience, 2011, 4, 359-362.	12.9	42
123	A ground-based observation of the LCROSS impact events using the Subaru Telescope. Icarus, 2011, 214, 21-29.	2.5	3
124	<i>EPOXI</i> : COMET 103P/HARTLEY 2 OBSERVATIONS FROM A WORLDWIDE CAMPAIGN. Astrophysical Journal Letters, 2011, 734, L1.	8.3	96
125	A pressure measurement method for highâ€ŧemperature rock vapor plumes using atomic line broadening. Journal of Geophysical Research, 2010, 115, .	3.3	6
126	Impact-induced N2 production from ammonium sulfate: Implications for the origin and evolution of N2 in Titan's atmosphere. Icarus, 2010, 209, 715-722.	2.5	21

#	Article	IF	CITATIONS
127	A hydrocode calculation coupled with reaction kinetics of carbon compounds within an impact vapor plume and its implications for cometary impacts on Galilean satellites. Icarus, 2010, 210, 411-423.	2.5	9
128	Interpretation on Deep Impact results: Radial distribution of ejecta and the size distribution of large-sized grains. Earth, Planets and Space, 2010, 62, 13-16.	2.5	1
129	Impact experiments with a new technique for acceleration of projectiles to velocities higher than Earth's escape velocity of 11.2 km/s. Journal of Geophysical Research, 2010, 115, .	3.3	15
130	Inâ€situ spectroscopic observations of silicate vaporization due to >10 km/s impacts using laser driven projectiles. Geophysical Research Letters, 2010, 37, .	4.0	9
131	Rotational-Temperature Measurements of Chemically Reacting CN Using Band-Tail Spectra. Journal of Thermophysics and Heat Transfer, 2009, 23, 463-472.	1.6	11
132	An empirical model for transient crater growth in granular targets based on direct observations. Icarus, 2009, 203, 310-319.	2.5	20
133	Farside Gravity Field of the Moon from Four-Way Doppler Measurements of SELENE (Kaguya). Science, 2009, 323, 900-905.	12.6	169
134	Direct measurements of chemical composition of shock-induced gases from calcite: an intense global warming after the Chicxulub impact due to the indirect greenhouse effect of carbon monoxide. Earth and Planetary Science Letters, 2009, 282, 56-64.	4.4	35
135	Efficient cyanide formation due to impacts of carbonaceous bodies on a planet with a nitrogenâ€rich atmosphere. Geophysical Research Letters, 2009, 36, .	4.0	17
136	Nonstop Mars Sample Return System Using Aerocapture Technologies. , 2009, , .		25
137	IMPACT EXPERIMENTS WITH PROJECTILES AT VELOCITIES HIGHER THAN 10 KMâ^•S. , 2009, , .		0
138	Subaru/COMICS Mid-Infrared Spectroscopic Observations of the Dust Plume from Comet 9P/Tempel. Globular Clusters - Guides To Galaxies, 2009, , 131-136.	0.1	0
139	The Subsurface Structure of Comet 9P/Tempel 1 Projected into the Dust Plume. Globular Clusters - Guides To Galaxies, 2009, , 143-146.	0.1	0
140	One Month of Near-IR Imaging Photometry of Comet 9P/Tempel 1. Globular Clusters - Guides To Galaxies, 2009, , 323-328.	0.1	1
141	The role of organic haze in Titan's atmospheric chemistry. Icarus, 2008, 194, 201-211.	2.5	39
142	The role of organic haze in Titan's atmospheric chemistry. Icarus, 2008, 194, 186-200.	2.5	63
143	Hydrodynamical and radiative transfer modeling of meteoroid impacts into Saturn's rings. Icarus, 2008, 194, 623-635.	2.5	12
144	Direct measurements of impact devolatilization of calcite using a laser gun. Geophysical Research Letters, 2008, 35, .	4.0	18

#	Article	IF	CITATIONS
145	Felsic highland crust on Venus suggested by Galileo Nearâ€Infrared Mapping Spectrometer data. Journal of Geophysical Research, 2008, 113, .	3.3	86
146	Impact vaporization of rocks using a high-power laser. Journal of Physics: Conference Series, 2008, 112, 042014.	0.4	2
147	The Thickness and Formation Age of the Surface Layer on Comet 9P/Tempel 1. Astrophysical Journal, 2007, 661, L89-L92.	4.5	28
148	The chemical composition of the early terrestrial atmosphere: Formation of a reducing atmosphere from CI-like material. Journal of Geophysical Research, 2007, 112, .	3.3	83
149	Thermal alteration of hydrated minerals during hypervelocity capture to silica aerogel at the flyby speed of Stardust. Meteoritics and Planetary Science, 2007, 42, 357-372.	1.6	56
150	Spectroscopic measurements of Si-O recombination process in laser-induced quartz vapor plumes. Earth, Planets and Space, 2007, 59, 437-451.	2.5	1
151	Non-intrusive measurements of crater growth. Icarus, 2007, 188, 506-521.	2.5	38
152	An experimental study on Fischer-Tropsch catalysis: Implications for impact phenomena and nebular chemistry. Meteoritics and Planetary Science, 2006, 41, 715-729.	1.6	23
153	The role of ricochet impacts on impact vaporization. International Journal of Impact Engineering, 2006, 33, 771-780.	5.0	21
154	The role of Fischer-Tropsch catalysis in Jovian subnebular chemistry. Astronomy and Astrophysics, 2006, 459, 965-968.	5.1	5
155	The role of Fischer–Tropsch catalysis in the origin of methane-rich Titan. Icarus, 2005, 178, 154-164.	2.5	32
156	Velocity distributions of high-velocity ejecta from regolith targets. Icarus, 2005, 178, 264-273.	2.5	15
157	Subaru Telescope Observations of Deep Impact. Science, 2005, 310, 274-278.	12.6	107
158	Deep Impact: Observations from a Worldwide Earth-Based Campaign. Science, 2005, 310, 265-269.	12.6	182
159	Evaluation of mineralogical alteration of micrometeoroid analog materials captured in aerogel. Advances in Space Research, 2004, 34, 2299-2304.	2.6	23
160	Laboratory experiments of Titan tholin formed in cold plasma at various pressures: implications for nitrogen-containing polycyclic aromatic compounds in Titan haze. Icarus, 2004, 168, 344-366.	2.5	284
161	Real-time detector for hypervelocity microparticles using piezoelectric material. Advances in Space Research, 2004, 34, 935-938.	2.6	22
162	Sulfur chemistry in laser-simulated impact vapor clouds: implications for the K/T impact event. Earth and Planetary Science Letters, 2004, 218, 347-361.	4.4	22

#	Article	IF	CITATIONS
163	Interactions between impact-induced vapor clouds and the ambient atmosphere: 1. Spectroscopic observations using diatomic molecular emission. Journal of Geophysical Research, 2003, 108, .	3.3	16
164	Interactions between impact-induced vapor clouds and the ambient atmosphere: 2. Theoretical modeling. Journal of Geophysical Research, 2003, 108, .	3.3	17
165	Methane production by large iron meteorite impacts on early Earth. Journal of Geophysical Research, 2003, 108, .	3.3	32
166	On observing the compositional variability of the surface of Venus using nightside near-infrared thermal radiation. Journal of Geophysical Research, 2003, 108, .	3.3	50
167	Intensities of atomic lines and molecular bands observed in impact-induced luminescence. Journal of Geophysical Research, 2003, 108, .	3.3	40
168	FEM analysis of current limiting characteristics of a superconducting thin film current limiting device by the current vector potential method. IEEE Transactions on Applied Superconductivity, 2003, 13, 2020-2023.	1.7	16
169	Response of Piezoelectric Lead–Zirconate–Titanate to Hypervelocity Silver Particles. Japanese Journal of Applied Physics, 2003, 42, 1496-1497.	1.5	13
170	Vapor clouds generated by laser ablation and hypervelocity impact. Geophysical Research Letters, 2002, 29, 40-1-40-4.	4.0	22
171	Initiation of Run-Out Flows on Venus by Oblique Impacts. Icarus, 2002, 155, 265-284.	2.5	30
172	Spectroscopic characterization of hypervelocity jetting: Comparison with a standard theory. Journal of Geophysical Research, 1999, 104, 30825-30845.	3.3	42
173	Spectroscopic measurements of vapor clouds due to oblique impacts. Journal of Geophysical Research, 1998, 103, 19427-19441.	3.3	66
174	Evolution of lunar topography by impact processes. Geophysical Research Letters, 1991, 18, 2125-2128.	4.0	1
175	Development of a realtime detector to hypervelocity microparticles using PZT ceramics. , 0, , .		0